JOURNAL OF CATALYSIS 154, 11–23 (1995)

On the Nature of the Active Species in Cesium-Doped V_2O_5–Fe_2O_3 Catalysts

A. Brückner,*,[1] G.-U. Wolf,* M. Meisel,† R. Stösser,† H. Mehner,‡ F. Majunke,§ and M. Baerns§

*Institut für Angewandte Chemie Adlershof, Rudower Chaussee 5, Haus 4.1, D-12484 Berlin, Germany; †Humboldt-Universität zu Berlin, Fachbereich Chemie, Hessische Straße 1-2, D-10115 Berlin, Germany; ‡Bundesanstalt für Materialforschung und-prüfung, Rudower Chaussee 5, D-12484 Berlin, Germany; and §Ruhr-Universität Bochum, Lehrstuhl für Technische Chemie,D-44780 Bochum, Germany

Received April 11, 1994; revised February 3, 1995

ESR studies of unsupported V_2O_5–Fe_2O_3 catalysts revealed that a new phase is formed by doping the solids with cesium sulfate. The percentage of this phase increases with increasing iron content. As indicated by XRD and Mössbauer spectra, the new phase is amorphous. Its composition is nonstoichiometric and varies slightly depending on the iron content. For catalysts with an atomic ratio of V : Fe : Cs = 1 : 1 : 0.06 and 1 : 1.4 : 0.06, approximate formal compositions of $Fe_{0.70}VO_{3.04}$ and $Fe_{0.65}VO_{3.14}$, respectively, were calculated. The new phase contains Fe^{3+} ions with oxygen lattice vacancies in their coordination sphere being occupied by an electron. Since the 9-fluorenone selectivity is improved drastically on cesium doping and with increasing iron content it seems likely that in addition to the diminished surface acidity these vacancies serve as active centres in the catalytic gas phase oxidation of fluorene. © 1995 Academic Press, Inc.

INTRODUCTION

The selective gas-phase oxidation of polycyclic aromatic hydrocarbons is of considerable scientific and industrial importance. Various V_2O_5-based catalysts have been used in these reactions. In the case of anthracene and fluorene, the selectivity of the inner-ring-oxidation products, 9,10-anthraquinone and 9-fluorenone, respectively, was slightly enhanced by increasing the Fe_2O_3 content of the catalyst (1). However, very high selectivities of up to 99% could be achieved when the oxidation was performed with V_2O_5–Fe_2O_3 catalysts doped with cesium sulfate. For explaining this effect various reasons have been discussed; in particular, the changes in the acid–base properties of the catalyst surface caused by alkali doping have been suggested as the reason for the increase in selectivity (2). It was assumed that the decrease in Lewis-acid sites weakens the adsorptive bonding of the basic hydrocarbons to the surface and, thus, diminishes the total oxidation probability.

[1] To whom correspondence should be addressed.

However, until now the nature of the catalytically active sites is not clear. The aim of this work is to obtain new results in this field. Therefore it is focused mainly on ESR studies since this method can provide detailed information on the local environment of paramagnetic centres and the magnetic interactions between them. The catalysts were treated at various temperatures and atmospheres during the recording of the ESR spectra. In addition, the samples were exposed to light of different wavelengths and high mechanical pressures. These *in situ* ESR studies gave indications of local structural changes in the catalyst phases induced by thermal and redox processes. Additional XPS, XRD, and Mössbauer measurements were performed to examine the phase composition. On the basis of all these results, conclusions about the probable active species in the cesium-doped V_2O_5–Fe_2O_3 catalysts were drawn.

METHODS

1. Catalyst Preparation

Catalysts with atomic ratios of V : Fe = 1 : 0.13, 1 : 1, and 1 : 1.4 were prepared from mixed solutions of ammonium vanadate in water and iron oxide in diluted HCl by coprecipitation with ammonia. For doping, Cs_2SO_4 was added to the solutions. The precipitate was filtered off, dried at 393 K, and calcined for 12 h at 623 or 773 K. The catalyst V : Fe = 1 : 0.74 was prepared according to the wet synthesis of $FeVO_4$ (3, 4) by precipitation of an aqueous solution containing ammonium vanadate and $Fe(NO_3)_3$ with ammonia. For doping, the precipitate calcined at 623 K was impregnated with Cs_2SO_4 solution and dried.

2. Catalyst Characterization

Specific surface areas were determined by the 1-point BET method using low temperature adsorption of N_2 (77 K) after the catalyst had been calcined in N_2 at 573 K

0021-9517/95 $6.00

for 2 h (5). The surface composition and the valence states of the cations were determined by XPS with Al$K\alpha$ radiation (Leybold/Heraeus AG LHS 10 spectrometer). After nonlinear background subtraction the spectra were fitted applying Gauss–Lorentz functions and the sensitivity factors of Wagner *et al.* (6).

The electrical conductivity of the catalysts was determined by measuring the resistance of the series Pt–electrode | sample | Pt–electrode with an AC measuring device (Wayne Kerr, type B905) using a special apparatus (7).

Crystalline components of the powdered catalysts were identified by XRD with Cu$K\alpha$ radiation.

ESR spectra were recorded with the ERS 300 and ERS 200 cw-spectrometers (Zentrum für Wissenschaftlichen Gerätebau, Berlin) in X- and Q-band, respectively, and with the E 4 cw-spectrometer (Varian) in X-band. The magnetic field was measured with reference to a standard of 2,2-diphenyl-1-picrylhydrazyl hydrate (DPPH). Relative line intensities were obtained according to $I_{rel} = A(\Delta B_{pp})^2$ where A is the peak-to-peak amplitude and ΔB_{pp} is the peak-to-peak linewidth (8). Computer simulation of the Fe^{3+} ESR spectra was based on the spin Hamiltonian

$$\begin{aligned}\mathbf{H} = {} & \beta \cdot \mathbf{S} \cdot \mathbf{g} \cdot \mathbf{B}_0 + D[\mathbf{S}_z^2 - \tfrac{1}{3}S(S+1)] + E[\mathbf{S}_x^2 - \mathbf{S}_y^2] \\ & + \tfrac{1}{6}a[\mathbf{S}_x^4 + \mathbf{S}_y^4 + \mathbf{S}_z^4 - \tfrac{1}{5}S(S+1)(3S^2+3S-1)] \\ & + \tfrac{1}{180}F[35\mathbf{S}_z^4 - 30S(S+1)\mathbf{S}_z^2 + 25\mathbf{S}_z^2 - 6S(S+1) \\ & + 3S^2(S+1)^2],\end{aligned} \quad [1]$$

where $S = 5/2$, β is the Bohr magneton, $\mathbf{S}$ is the total spin operator, $\mathbf{g}$ is the g-tensor, $\mathbf{B}_0$ is the magnetic field vector, $\mathbf{S}_x$, $\mathbf{S}_y$, and $\mathbf{S}_z$, respectively, are the spin matrices, a and F are the cubic field splitting constants, and D and E are the zero-field parameters which describe the deviation of the Fe^{3+} coordination sphere from cubic symmetry (9). For the simulation of V^{4+} signals ($S = 1/2$) only the term $\beta \cdot \mathbf{S} \cdot \mathbf{g} \cdot \mathbf{B}_0$ had to be taken into account. The variation of temperature (93 K $< T <$ 423 K) was carried out with a TEL 2 temperature control unit (Zentrum für Wissenschaftlichen Gerätebau, Berlin). In the range 298 K $<$ T $<$ 823 K, the ER 4114 HT high temperature cavity (Bruker) was used. *In situ* irradiation of the samples was done with a 500 W mercury high-pressure lamp (NARVA, Berlin). Pressure-dependent *in situ* ESR measurements were performed with a home-made pressure device consisting of a Plexiglas sample chamber which was placed between two quartz pistons within the cavity. The pressure was generated by a hydraulic system. The effective pressure at the sample, p_2, was calculated according to $p_2 = p_1A_1/A_2$, where p_1 is the pressure applied to the piston of the hydraulic system measured using an oil manometer, A_1 is the area of the hydraulic piston, and A_2 is the area of the small quartz piston within the sample chamber.

Mössbauer spectra were recorded using an SM 2201 spectrometer (Internauc Pribor, Leningrad) equipped with a ^{57}Co source in zero field at 300 K. All isomer shifts are quoted relative to an absorber of metallic iron at room temperature. Parameter fits were performed using a standard least-squares fitting routine.

3. *Catalytic Experiments*

Fluorene had been oxidized with air in an electrically heated, nearly isothermal fixed-bed quartz reactor (d = 0.8 cm, l = 30 cm), which was described previously (10).

The product distribution obtained in the oxidation experiments was determined by GC (Sichromat 2 gas chromatograph, Siemens) and HPLC analysis (Waters 712 UV array detector). For details of the product analysis see Ref. (11).

RESULTS

In this section the results of phase characterization and catalytic behaviour of various pure and cesium-doped V_2O_5–Fe_2O_3 catalysts are described. The catalyst characterization was mainly focused on *in situ* ESR investigations under various temperatures and atmospheres, under high mechanical pressure, and under irradiation with light. These experiments gave indications as to the nature of the active centres.

1. Catalyst Characterization

The catalysts were characterized with respect to their BET surface, surface composition, surface acidity, oxygen chemisorption (Table 1), phase composition (Table 2), and electrical conductivity (Figs. 1 and 2, Table 3). XPS measurements revealed that cesium is preferably enriched in the catalyst surface. This effect is enhanced as the iron content of the catalyst increases. In contrast, the amount of iron on the surface is lowered for both the doped and the undoped catalyst (Table 1). On the other hand, increasing iron content weakens the surface acidity. The intensity of the IR bands corresponding to pyridine adsorption on the Lewis and Brønsted sites is diminished (Table 1). By doping with cesium, the surface acidity is reduced even more drastically. Therefore, and in consequence of the low specific surface areas, in some cases the intensity of the appropriate pyridine IR adsorption bands was too low to be evaluated properly (Table 1).

The amount of oxygen chemisorbed at 623 K was determined by GC pulse chromatography after reducing the catalyst with hydrogen at the same temperature. The oxygen uptake increases remarkably when the samples were

TABLE 1

Surface Properties of the Various Catlysts: BET Surface, S_{BET} (m^2/g), XPS Surface Composition (Fe : Cs Atomic Ratio Calculated for V = 1), IR-Intensities of Pyridine Adsorption Bands for Lewis Sites (1450 cm^{-1}) and Brønsted Sites (1540 cm^{-1}) and Oxygen Uptake (μmol O_2/m^2) According to the GC Pulse Method

Bulk composition V : Fe : Cs atomic ratio	S_{BET} (m^2/g)	Surface composition, atomic ratio (V^{5+} = 1)		Lewis sites at 1450 cm^{-1} (area units)	Brønsted sites at 1540 cm^{-1} (area units)	Oxygen uptake (μmol O_2/m^2)
		Fe^{3+}	Cs^+			
1 : 0.13 : 0	6.1	0.15	0	0.8	—	169 ± 28
1 : 0.13 : 0.06	4.1	0.04	0.05	—	—	44 ± 5
1 : 0.74 : 0[a]	25.1	0.68	0	1.8	0.5	36 ± 3
1 : 0.74 : 0.06[a]	19.9	0.70	0.19	1.1	—	27 ± 3
1 : 1 : 0	3.5	0.42	0	—	—	134 ± 15
1 : 1 : 0.06	1.7	0.83	0.73	—	—	198 ± 18
1 : 1.4 : 0	1.3	0.76	0	—	—	190 ± 15
1 : 1.4 : 0.06	3.6	0.60	0.38	0.2	0.3	531 ± 30

[a] Prepared by wet synthesis of $FeVO_4$.

TABLE 2

Phase Composition of the Catalysts, Relative Amount of Iron Containing Components with Respect to the Overall Iron Content of the Catalyst, A_{Fe} (%), Determined by Mössbauer Spectra, Effective g-Value (g') and Peak-to-Peak Line Width, ΔB_{pp} (mT) of the ESR Signals

Bulk composition V : Fe : Cs	Phase composition	A_{Fe} (%)	g'	ΔB_{pp} (mT)
1 : 0.13 : 0	V_2O_5 (main component)[a]			
	$Fe_2V_4O_{13}$[a]	61	≈2	51.5
	Amorphous phase	39	≈2	51.5
1 : 0.13 : 0.06	V_2O_5 (main component)[a]			
	$Fe_2V_4O_{13}$[a]	30	≈2	Superposition
	Amorphous phase	70	1.948	
1 : 0.74 : 0[b]	$FeVO_4$[a]	75	≈2	83.3
	Amorphous phase	25	≈2	83.3
1 : 0.74 : 0.06[b]	$FeVO_4$[a]	75	≈2	80.8
	Amorphous phase	25	≈2	80.8
	$Fe_xV_yO_z$	Trace	≈18	36.0
1 : 1 : 0	$FeVO_4$[a]	100	≈2	129.9
1 : 1 : 0.06	$FeVO_4$[c]	Trace	≈2	58.8
	$Fe_2V_4O_{13}$[a]	39	≈2	58.8
	α-Fe_2O_3[a]	45	—	—
	$Fe_xV_yO_z$	16	≈18	32.0
1 : 1.4 : 0	$FeVO_4$[a]	69	≈2	130.0
	α-Fe_2O_3[a]	31	—	—
1 : 1.4 : 0.06	$FeVO_4$[a]	32	≈2	130.0
	α-Fe_2O_3[a]	42	—	—
	$Fe_xV_yO_z$	26	≈18	41.7
$FeVO_4$			≈2	134.8
$Fe_2V_4O_{13}$			≈2	57.6

[a] Crystalline components identified by XRD.
[b] Prepared by wet synthesis of $FeVO_4$.

TABLE 3

Exponent n of the Conductivity Dependence on Oxygen Partial Pressure (Eq. [2]) for the Cesium-Doped and the Cesium-Free Catalyst V : Fe = 1 : 1.4

	T (K)				
Catalyst	573	598	623	648	673
Cs-free	2.3	2.4	2.5	2.7	2.8
Cs-doped	4.5	4.9	5.4	5.6	5.8

doped with cesium, except those having low V : Fe ratios of 1 : 0.13 and 1 : 0.74, respectively (Table 1).

The bulk phase composition of the catalysts, as derived from XRD spectra for crystalline components as well as from ESR and Mössbauer spectra, is presented in Table 2. In due course, special attention is paid to the ESR measurements which clearly show differences in the catalyst composition caused by cesium doping.

The electrical conductivity σ has been measured for the iron-rich catalyst V : Fe = 1 : 1.4 at different temperatures and oxygen partial pressures (Fig. 1). σ increases with temperature for both the cesium-free and the cesium-doped catalyst. However, for the latter, σ is lower than for the former. In addition, from Fig. 1 it can be seen that σ decreases with increasing oxygen partial pressure. This indicates that both the doped and the undoped catalysts are n-type semiconductors (12). For such compounds, adsorbed oxygen is assumed to capture electrons from the conduction band, thus lowering the conductivity. For oxygen partial pressures above 1 kPa, there exists a linear correlation between log σ and log $P(O_2)$. From this, the exponent n of the conductivity dependence on the oxygen pressure can be calculated using the equations

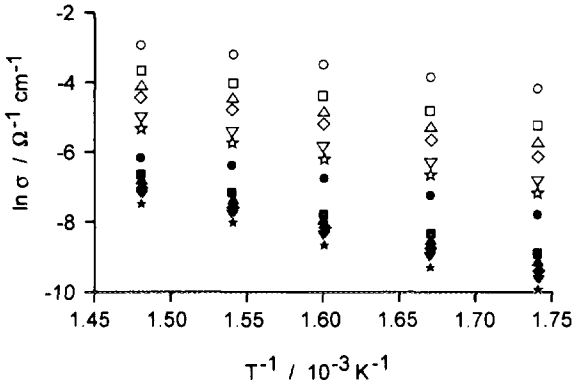

FIG. 1. Electrical conductivity, σ, as a function of temperature for the catalysts V : Fe : Cs = 1 : 1.4 : 0 (filled symbols) and V : Fe : Cs = 1 : 1.4 : 0.06 (open symbols) at different oxygen partial pressures; ((●) 0.01 kPa, (■) 1.00 kPa, (▲) 3.16 kPa, (◆) 10.00 kPa, (▼) 31.60 kPa, (★) 100.00 kPa).

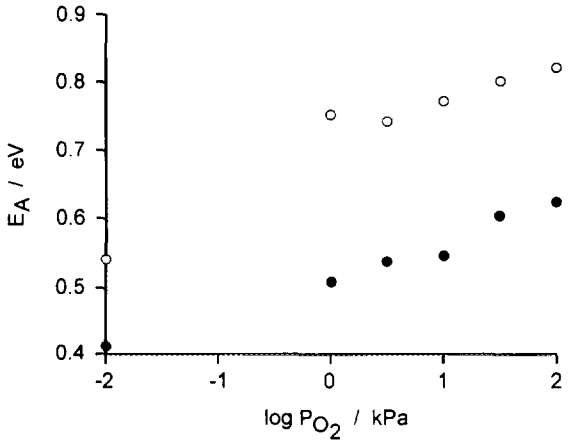

FIG. 2. Activation energy of the electrical conduction, E_A, as a function of oxygen partial pressure for the catalysts V : Fe : Cs = 1 : 1.4 : 0 (filled circles) and V : Fe : Cs = 1 : 1.4 : 0.06 (open circles).

$$\sigma = k \cdot P(O_2)^{-1/n} \quad \text{with } -1/n = \log \sigma / \log P(O_2). \qquad [2]$$

The exponent n indicates how many electrons are transferred from the catalyst to the oxygen molecule according to

$$\tfrac{1}{2}O_2 + 2e^- \rightarrow O^{2-} \quad \sigma = k \cdot P(O_2)^{\pm 1/4} \qquad [3]$$

$$\tfrac{1}{2}O_2 + e^- \rightarrow O^- \quad \sigma = k \cdot P(O_2)^{\pm 1/2} \qquad [4]$$

$$O_2 + e^- \rightarrow O_2^- \quad \sigma = k \cdot P(O_2)^{\pm 1}. \qquad [5]$$

For the cesium-free catalyst V : Fe = 1 : 1.4, n takes values between 2 and 3 (Table 3). In the case of the doped sample, n is between 4 and 6 (Table 3). This suggests that the undoped catalyst absorbs oxygen in the form of O^- whereas the cesium-containing solid preferably adsorbs O^{2-}. From the slope of the conductivity dependence on temperature (Fig. 1), the activation energy of the electrical conduction can be deduced according to the Arrhenius equation

$$\ln \sigma = \ln \sigma_0 + (E_A/RT). \qquad [6]$$

E_A rises with increasing oxygen partial pressure for both catalysts (Fig. 2). However, at a given oxygen pressure, E_A for the cesium-free compound is lower than for the doped one.

2. ESR Measurements

2.1. *Cesium-Free V_2O_5–Fe_2O_3 Catalysts*

In the ESR spectra of the undoped catalysts at room temperature, only a broad signal at $g' \approx 2$ appeared (Table 2). It is caused by Fe^{3+} ions with small zero-field splittings in a relatively symmetrical environment of oxide ions. The large linewidth arises from dipole–dipole inter-

actions between neighbouring spins. The signal assignment is verified by comparing the ESR spectra with those of the reference substances $FeVO_4$ and $Fe_2V_4O_{13}$, as well as on the basis of the phase compositions derived from XRD and Mössbauer data (Table 2).

For the iron-rich samples V : Fe = 1 : 1 and 1 : 1.4, the ESR linewidth agrees well with that of $FeVO_4$. The assignment is also confirmed by the Mössbauer spectra, the only signals of which originate from $FeVO_4$ and a mixture of $FeVO_4$ and α-Fe_2O_3, respectively (Fig. 3). Since the latter is antiferromagnetic at room temperature it does not contribute to the ESR spectrum.

The catalysts V : Fe = 1 : 0.13 and 1 : 0.74 with lower iron contents differ from the reference substances $FeVO_4$ and $Fe_2V_4O_{13}$ with respect to the ESR linewidth. In the XRD spectra no other crystalline, iron-containing compound was observed apart from $Fe_2V_4O_{13}$ and $FeVO_4$, respectively. Hence, the difference in the ESR linewidth must be due to an additional amorphous phase. In the Mössbauer spectra (Fig. 3), this phase is represented by the two doublets with the larger quadrupole splitting which superimpose the signals originating from $FeVO_4$ in

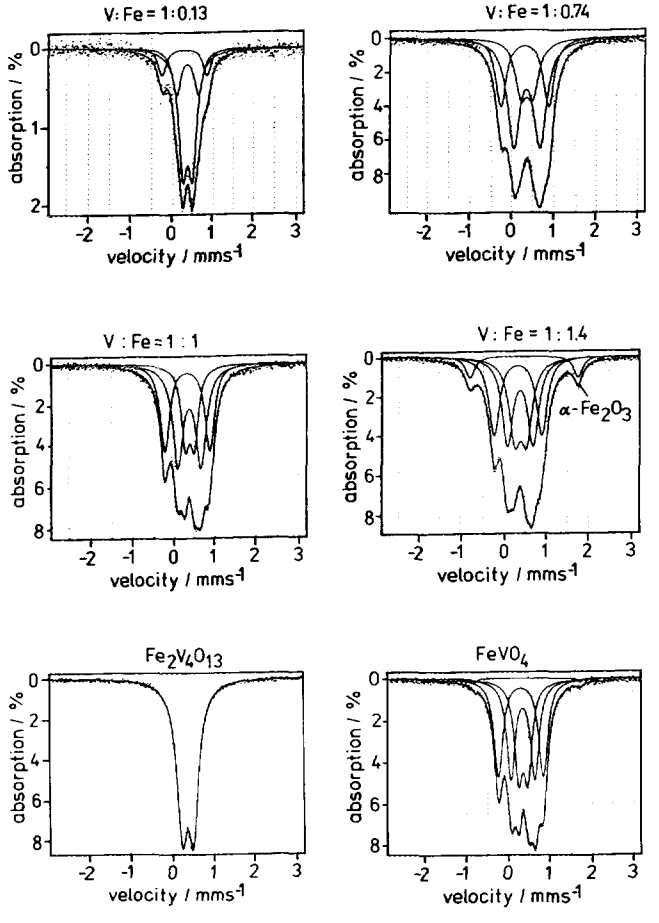

FIG. 3. Mössbauer spectra of undoped catalysts and reference samples, $FeVO_4$ and $Fe_2V_4O_{13}$.

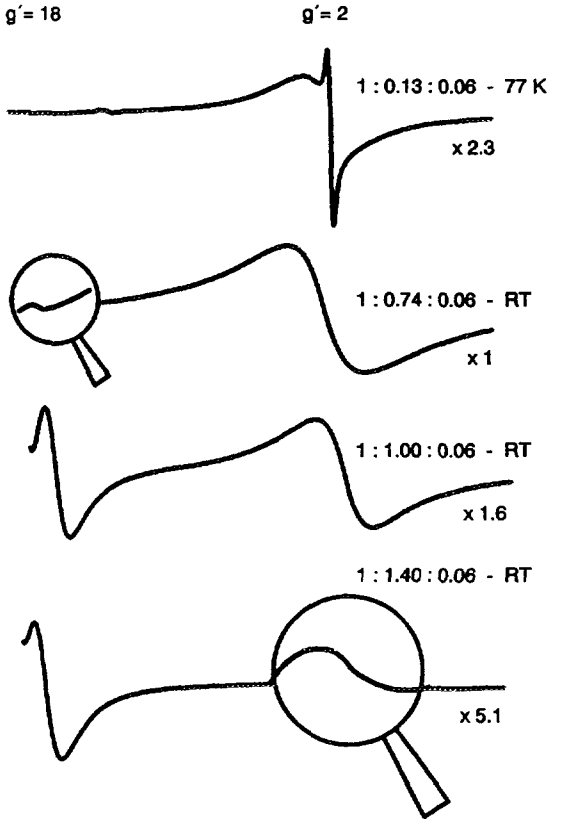

FIG. 4. ESR spectra of cesium-doped catalysts.

sample V : Fe = 1 : 0.74. Therefore, the two outer doublets in this spectrum appear with higher intensity than expected for pure $FeVO_4$. In V : Fe = 1 : 0.13 these doublets arise in addition to the signal of $Fe_2V_4O_{13}$.

2.2. *Cesium-Doped V_2O_5–Fe_2O_3 Catalysts*

Cesium-doped catalysts have also a broad ESR signal at $g' \approx 2$ (Table 2, Fig. 4). In the iron-poor sample V : Fe : Cs = 1 : 0.13 : 0.06, it arises from $Fe_2V_4O_{13}$ and is superimposed by a narrow line at $g' = 1.948$. At 77 K a better resolution is achieved due to the broadening of the $Fe_2V_4O_{13}$ signal. The g-value of 1.948 is characteristic for V^{4+} (13). The narrow linewidth points to an effective spin–spin exchange interaction between neighbouring V^{4+} centres. This signal is ascribed to an amorphous Fe^{3+}–V^{4+}–O phase. In the corresponding Mössbauer spectrum it causes three doublets in addition to that of $Fe_2V_4O_{13}$ (Fig. 5).

For sample V : Fe : Cs = 1 : 0.74 : 0.06, neither the ESR nor the Mössbauer spectra differ from those of the undoped catalyst. Therefore, assignment of the signals corresponds to the cesium-free sample.

The $g' \approx 2$ lines of the iron-rich catalysts V : Fe : Cs = 1 : 1 : 0.06 and 1 : 1.4 : 0.06 are caused by $Fe_2V_4O_{13}$ and $FeVO_4$, respectively, as indicated by the agreement of

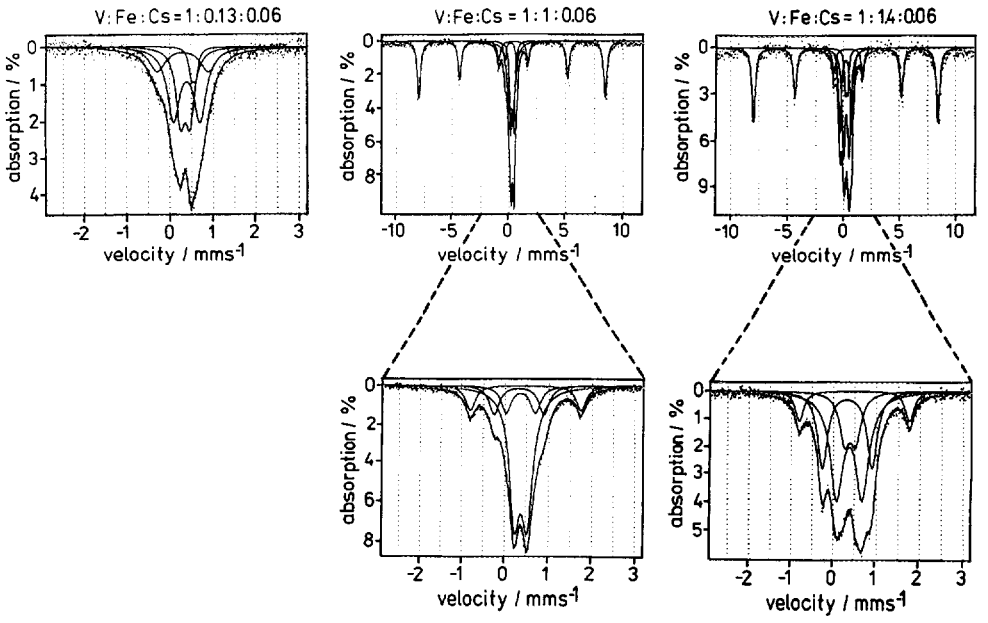

FIG. 5. Mössbauer spectra of cesium-doped catalysts.

the ESR linewidth with that of the reference samples. This assignment is verified by the fact that $Fe_2V_4O_{13}$ and $FeVO_4$, respectively, are the main components of the Mössbauer spectra apart from α-Fe_2O_3 (Fig. 5). With increasing iron content of the samples, an additional line at very low resonant field values (B_0 = 32 mT, $g' \approx 18$) appears (Fig. 4). In sample V : Fe : Cs = 1 : 0.74 : 0.06 it is hardly visible but it gains intensity as the iron content increases. The $g' \approx 18$ signal is not evident in cesium-doped iron oxide precipitated in the same manner as the catalysts but without adding ammonium vanadate. Hence, the phase represented by this signal most likely contains iron and vanadium as well and should be regarded as $Fe_xV_yV_z$. In the XRD spectra no other reflections were observed in addition to those of α-Fe_2O_3, $Fe_2V_4O_{13}$, and $FeVO_4$, respectively. This indicates that the new phase is amorphous. In the Mössbauer spectra (Fig. 5) $Fe_xV_yO_z$ gives rise to two doublets. In sample V : Fe : Cs = 1 : 1 : 0.06 they appear in addition to that of $Fe_2V_4O_{13}$ and in V : Fe : Cs = 1 : 1.4 : 0.06 they superimpose the two outer doublets of $FeVO_4$. The sextet for α-Fe_2O_3 covers a much larger velocity range than the signals of the other components. Therefore, two spectra in different velocity sections were recorded for the α-Fe_2O_3-containing catalysts in order to get careful parameter fits for all components. From the relative signal areas the percentage of the various iron-containing phases, with respect to the overall iron content of the catalysts, was estimated (Table 2).

The $g' \approx 18$ ESR line of $Fe_xV_yO_z$ arises from axially distorted Fe^{3+} centres. Such centres give signals in the low field range if $h\nu/D \approx 2$ (14), where h is the Planck constant, ν is the microwave frequency (in X-band $\approx$ 9.5 GHz, in Q-band $\approx$ 35.0 GHz), and D is the zero-field splitting parameter, which is a measure of the axial distortion of the Fe^{3+} coordination sphere. By computer simulation of the powder spectrum of sample V : Fe : Cs = 1 : 1 : 0.06 a value of $|D/h|$ = 4800 MHz was obtained in the expected range (Fig. 6). In both the X-band and the Q-band a satisfactory fit of calculated and experimental spectra was achieved with the same parameter set, indicating that the zero-field values obtained for these centres reflect the local symmetry fairly well.

Temperature dependent ESR measurements revealed for V : Fe : Cs = 1 : 1 : 0.06 that the intensity of the $Fe_2V_4O_{13}$ signal at $g' \approx 2$ decreases with increasing temperature as expected for pure paramagnetic behaviour, according to the Curie–Weiss law (Fig. 7). In contrast, the $g' \approx 18$ line shows unexpected thermal behaviour. Its intensity increases with increasing temperature, reaching a maximum at about 300 K. At higher temperature the signal loses intensity, broadens, and finally vanishes at about 430 K. During this process it is shifted to higher field values ($g' \approx 6$). The observed temperature dependence and line position indicate an oxygen vacancy next to Fe^{3+} occupied by an electron, Fe^{3+}–$V_O(e^-)$. Such species were also observed in other oxidic systems, such as iron-doped $BaTiO_3$ (15). In contrast to Fe^{3+} ions with a saturated coordination sphere like those in $Fe_2V_4O_{13}$ or $FeVO_4$ ($g' \approx 2$), those next to an oxygen vacancy ($g' \approx 18$) should be easily influenced by temperature, oxygen atmosphere, mechanical stress, or photochemical activation. The following *in situ* ESR measurements under varying conditions were carried out to get more experimental evidence

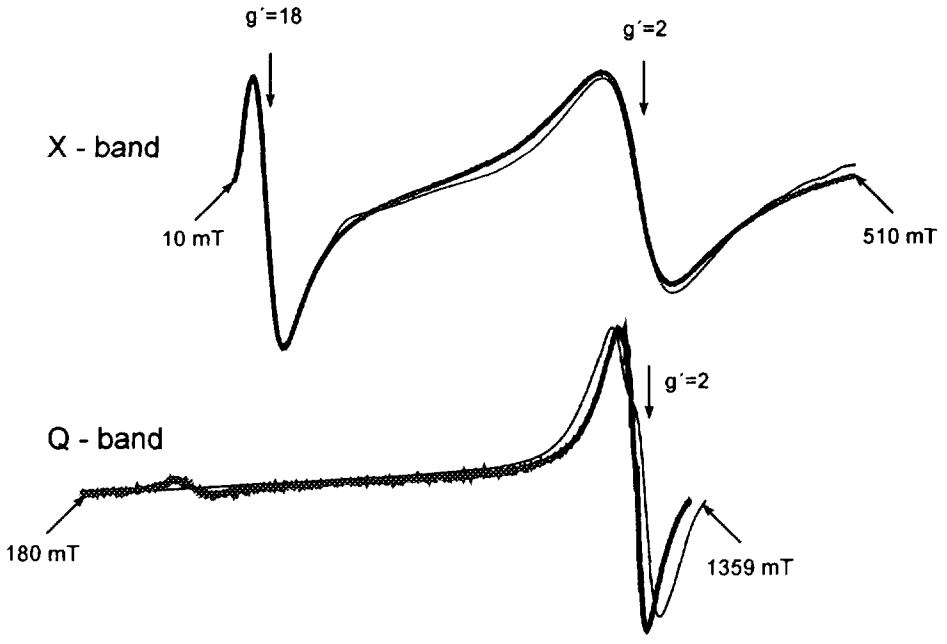

FIG. 6. Simulated (weak line) and experimental (bold line) ESR spectra of catalyst V : Fe : Cs = 1 : 1 : 0.06 at room temperature (calculation by superimposing five spectra with the following parameters: (i) $S = 5/2$, $g_{iso} = 2.00$, $D = 4800$ MHz, $a = 960$ MHz, $\Delta B = 10.0$ mT; (ii) $S = 5/2$, $g_{iso} = 2.00$, $D = 4000$ MHz, $a = 800$ MHz, $\Delta B = 50.0$ mT; (iii) $S = g_{iso} = 2.00$, $D = 3600$ MHz, $a = 720$ MHz; $\Delta B = 50.0$ mT; (iv) $S = 5/2$, $g_{iso} = 2.10$, $D = 0$, $a = 0$, $\Delta B = 55.0$ mT; (v) $S = 1/2$, $g_{iso} = 1.96$, $\Delta B = 25.0$ mT.

for the assignment of the $g' \approx 18$ signal to Fe^{3+}–$V_0(e^-)$. For these experiments the catalyst V : Fe : Cs = 1 : 1 : 0.06 was used in which both the $g' \approx 18$ and the $g' \approx 2$ line have similar peak-to-peak amplitudes (Fig. 4). Thus, changes in these signals caused by the variation of the above-mentioned conditions could be recorded simultaneously.

2.2.1. Behaviour of sample V : Fe : Cs = 1 : 1 : 0.06 during illumination with light. The 500 W mercury high-pressure lamp used in these experiments produces white light consisting of different wave lengths. The short wavelength part (UV) should, by photochemical activation, lead to the recombination of charge carriers in the solid. Therefore we expected that the $g' \approx 18$ signal would irreversibly disappear on illuminating the sample 1 : 1 : 0.06 with this lamp. However, the low field signal shows the same behaviour as observed for the temperature dependent measurements described above (Fig. 8). It broadens and is shifted to higher field values whereas the $g' \approx 2$ line remains nearly unaffected. These reversible changes do not take place if a 435-nm filter is used to eliminate the long wavelength part of the light (IR) which is responsible for the activation of thermal lattice vibrations. Thus, it is clearly shown that the observed changes in the ESR spectrum are due to thermal activation caused by IR radiation. Photochemically (UV) induced recombination of charge carrier does not take place.

2.2.2. Thermal behaviour of sample V : Fe : Cs = 1 : 1 : 0.06 under various atmospheres and in vacuo. The

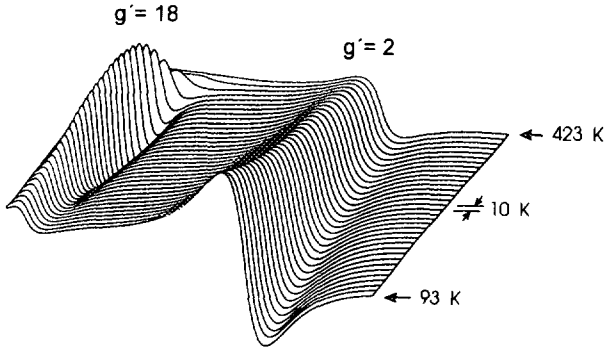

FIG. 7. Reversible temperature dependence of ESR spectrum of catalyst V : Fe : Cs = 1 : 1 : 0.06 in the range 93 K < T < 423 K.

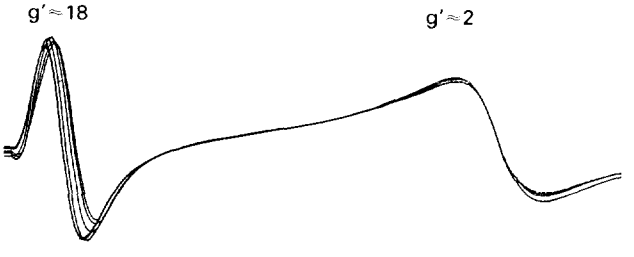

FIG. 8. Variation of ESR spectrum during illuminating catalyst V : Fe : Cs = 1 : 1 : 0.06 with white light.

temperature dependent changes of the ESR spectrum for V : Fe : Cs = 1 : 1 : 0.06 in the range 93 K < T < 423 K proved to be completely reversible (Fig. 7). To examine the influence of higher temperatures and of the atmosphere this sample was heated in a high temperature cavity under nitrogen and oxygen atmospheres, respectively, to the temperature shown in Fig. 9. After reaching the appropriate value the sample was cooled to room temperature and an ESR spectrum was recorded. At about 650 K the intensity of the low field signal starts to decrease irreversibly until it vanishes completely at about 800 K. This process is not influenced by the surrounding atmosphere. In contrast, the intensity of the $g' \approx 2$ signal depends strongly on whether the experiment is carried out under nitrogen or oxygen atmosphere. Obviously, the ESR spectrum of this sample is not only influenced by temperature and atmosphere but also by the calcination time (Table 4); heating the sample in a sealed tube over an extended period of time at a lower temperature also causes the $g' \approx 18$ signal to decrease irreversibly. Under oxygen atmosphere the $g' \approx 2$ line intensity increases by the same amount by which the $g' \approx 18$ line intensity is decreased as observed in the *in situ* experiment. *In vacuo* both signals loose intensity similar to the behaviour under nitrogen atmosphere.

2.2.3. Behaviour under mechanical stress. The following experiments were based on the assumption that the local symmetry of Fe^{3+} in the neighbourhood of a vacancy should be more easily influenced by external stress than Fe^{3+} in a saturated coordination sphere. Therefore, we exposed the sample V : Fe : Cs = 1 : 1 : 0.06 to a pressure of 2 GPa during the recording of the ESR spectrum. The intensity of the $g' \approx 18$ signal was reduced remarkably and another very broad line appeared in the range $g' > 2$ whereas the signal at $g' \approx 2$ remains unaffected. By removing the pressure, the initial spectrum can be reproduced, indicating that the structural changes are reversible (Fig. 10).

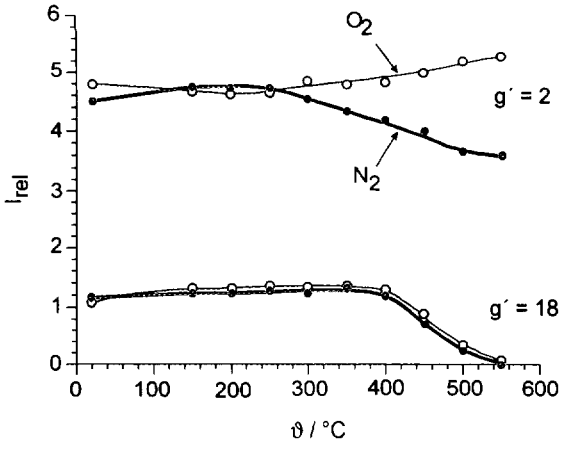

FIG. 9. Irreversible variation of relative ESR signal intensities at $g' \approx 2$ and $g' \approx 18$ for catalyst V : Fe : Cs = 1 : 1 : 0.06 after heating under oxygen or nitrogen atmosphere to the appropriate temperature and subsequent cooling to room temperature.

TABLE 4

Relative ESR Signal Intensities of the Catalyst V : Fe : Cs = 1 : 1 : 0.06 after Thermal Treatment in a Sealed Tube under Oxygen Atmosphere and *in Vacuo*

	I_{rel} ($g' \approx 18$)	I_{rel} ($g' \approx 2$)
Parent sample	0.28	1.24
2 h/623 K/O_2	0.011	1.52
2 h/623 K/Vacuo	0.016	0.85

2.2.4. Reaction with fluorene. The interaction of pure and cesium-doped catalysts V : Fe = 1 : 0.13 and V : Fe = 1 : 1.4, as well as of some reference samples with fluorene, was studied by ESR *in situ*. One-to-one (1 : 1) mixtures of catalyst and reactant were heated in sealed tubes in the absence of gaseous oxygen to probe the oxidative behaviour of the catalyst surface itself. A very narrow signal with a peak-to-peak linewidth of 0.6 mT appears over certain catalysts at higher temperatures. We attribute this line to a radical derived from fluorene. Hyperfine splitting is not resolved due to line broadening caused by magnetic interactions. Polyaromatic hydrocarbons like fluorene have low ionization potentials (fluorene: 8.36 eV) (16). Therefore, they can easily be oxidized to radicals or radical cations, particularly in the presence of transition metal ions (17). The relative intensities of the radical signal (Table 5) indicate that the radical formation is highest over catalysts exposing the $V^{5+} = O$ group to the surface (V_2O_5, β-$VOPO_4$). Since the composition V : Fe = 1 : 0.13 contains V_2O_5 as the main component, radical formation over this catalyst is comparable to that over pure V_2O_5. Pentavalent vanadium, which does not form a $V^{5+} = O$ bond ($FeVO_4$), and tetravalent vanadyl

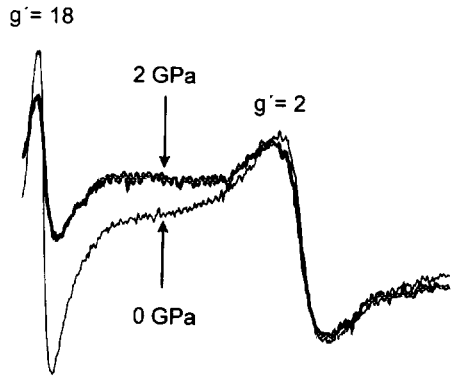

FIG. 10. Reversible change in the ESR spectrum of catalyst V : Fe : Cs = 1 : 1 : 0.06 under external mechanical pressure.

TABLE 5

Relative Intensity of the Radical Signal Formed during Reaction of Fluorene with Various Catalysts at Different Temperatures

Catalyst	T (K)								
	393	413	433	453	473	493	513	533	553
V_2O_5	0.10	0.08	0.11	0.20	0.60	1.52	4.03	9.58	16.15
β-$VOPO_4$	—	0.06	0.17	0.47	0.92	2.15	8.13	15.27	15.33
$FeVO_4$	—	—	—	—	—	—	—	0.10	0.11
$(VO)_2P_2O_7$	—	—	—	—	—	—	—	0.03	0.24
V : Fe : Cs = 1 : 0.13 : 0.06	0.26	0.37	0.43	0.61	1.07	2.20	4.80	8.25	9.90
V : Fe = 1 : 0.13	—	0.20	0.44	0.54	1.01	2.39	6.46	11.10	15.24
V : Fe : Cs = 1 : 1.4 : 0.06	—	—	—	—	—	—	—	0.11	0.32
V : Fe = 1 : 1.4	—	—	—	—	0.12	0.30	0.36	0.54	0.59

ions (in $(VO)_2P_2O_7$) seem not to have such strong oxidation properties that free radicals are formed to a considerable extent (Table 5). Similar results were obtained when both reactants in the sample tube were separated by a layer of quartz wool so that, on heating, fluorene sublimed and reacted with the catalyst surface as a gas.

3. Catalytic Results

All the V_2O_5–Fe_2O_3 compositions described above were tested in the catalytic gas-phase oxidation of fluorene. The possible reactions in this process are summarized in the following reaction scheme (2):

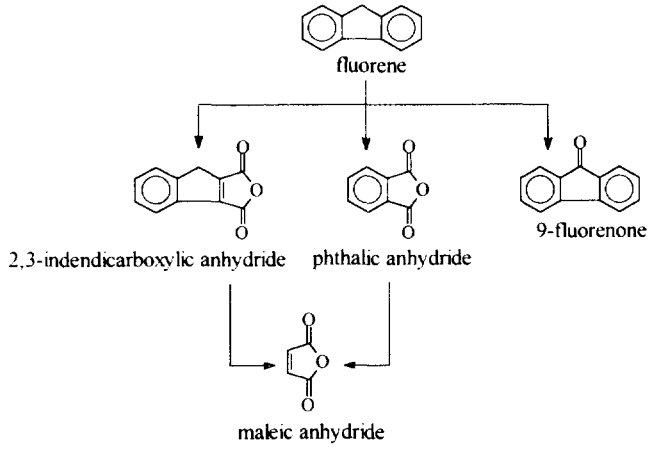

The aim of the catalyst design was to achieve 9-fluorenone selectivities as high as possible and to suppress nonselective oxidative destruction of the ring systems leading to phthalic anhydride, maleic anhydride, and the carbon oxides. It was found that the 9-fluorenone selectivity is enhanced for both the Cs_2SO_4-doped and the undoped phases when the iron content increases (Fig. 11). However, the most striking influence on the selectivity is exerted by cesium doping. The Cs-containing catalysts favour the selective oxidation of fluorene to 9-fluorenone remarkably. The catalyst consisting of V : Fe : Cs = 1 : 1.4 : 0.06 proved to have the best performance; a maximum selectivity of 99% was achieved (Fig. 11). Higher cesium contents did not lead to any further selectivity improvement. The 9-fluorenone selectivity for all doped and undoped catalysts studied does not depend on the degree of conversion between 20 and 90% of total conversion. At conversions above 90%, oxidative decomposition of 9-fluorenone to phthalic anhydride becomes significant. However, for the catalyst V : Fe : Cs = 1 : 1.4 : 0.06 having the best performance, 9-fluorenone selectivity is independent of total conversion, and no decomposition to phthalic anhydride, as occurred for the undoped catalyst, was observed (Fig. 12).

DISCUSSION

1. Characterization of the New $Fe_xV_yO_z$ Phase

The main difference in the ESR spectra of pure and the cesium-doped V_2O_5–Fe_2O_3 phases arises from the line at

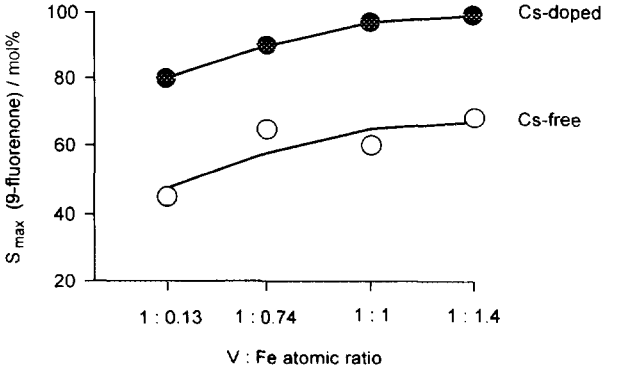

FIG. 11. Maximum 9-fluorenone selectivity, which is independent of degrees of total conversion between 20 and 90%, as a function of catalyst composition.

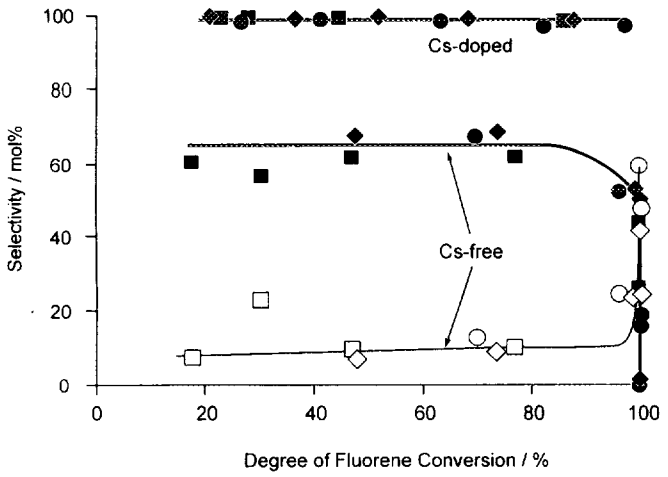

FIG. 12. Selectivity of 9-fluorenone (filled symbols) and phthalic anhydride selectivity (open symbols) as a function of the degree of conversion for the cesium-doped and the pure catalyst V : Fe = 1 : 1.4 at various reaction temperatures: (■) T = 623 K, (◆) T = 653 K, and (●) T = 673 K.

$g' \approx 18$ which appears exclusively when cesium is added to the solids. The signal is ascribed to an amorphous $Fe_xV_yO_z$ phase, the percentage of which depends on the iron content (Table 2). Moreover, a minimum iron content, which should be about 25% (corresponding to V : Fe : Cs = 1 : 0.74 : 0.06), seems to be necessary for the formation of this phase, although this value must be considered with caution due to differences in the sample preparation and cesium doping. The iron-poor phase V : Fe : Cs = 1 : 0.13 : 0.06, the main component of which is V_2O_5, does not show the $g' \approx 18$ signal. Possibly, the amorphous phase represented by $g' \approx 18$ needs an iron-containing carrier like α-Fe_2O_3, $Fe_2V_4O_{13}$, or $FeVO_4$ on which to be precipitated. This is also supported by the fact that the new phase is only formed in the presence of cesium, indicating that these large, easily polarizable cations probably stabilize the defect centres in it. XPS measurements showed that cesium is preferably localized on the surface of the catalyst (Table 1), so it seems likely that this new phase is distributed over the surface, too.

As already mentioned, the ESR line at $g' \approx 18$ is ascribed to a new phase which contains axially distorted Fe^{3+} centres (14), the distortion of which is caused by oxygen vacancies, V_O in their coordination sphere (15). Such Fe^{3+}–V_O centres have been frequently observed in other oxidic systems, for instance, in iron-doped perovskites. In these circumstances the vacancies are formed by removal of an oxygen atom from the FeO_6 octahedron, which causes a strong axial distortion of the Fe^{3+} environment, leading to $|D|$ values in the 30 GHz region (15, 18, 19). The zero-field parameter $|D|$ = 4800 MHz, which we obtained by computer simulation of the ESR powder spectrum (Fig. 6), is lower than that for Fe^{3+}–V_O centres in perovskites. The reason may be that in the V_2O_5–Fe_2O_3 catalysts the oxygen vacancy is not located in the first but in the second coordination sphere of the Fe^{3+} ion.

The temperature and pressure dependence of the $g' \approx 18$ signal strongly supports its assignment to Fe^{3+}–V_O centres. The reversible variation in the temperature range from 93 to 423 K can be explained by assuming that the vacancy is occupied by an electron (15). At low temperatures the unpaired electron interacts antiferromagnetically with the Fe^{3+} ion, partially compensating one of the five spins. Accordingly, the intensity of the signal decreases. In the high temperature range, thermal lattice vibrations gain influence. They alter the position of the vacancy slightly with respect to the Fe^{3+} ion. Thus, a distribution of the $|D|$ values is caused which broadens the $g' \approx 18$ signal until it disappears. In addition, the line is shifted to higher resonant field values ($g' \approx 6$) indicating that $|D|$ increases and the Fe^{3+} ion moves toward the vacancy. This effect was also observed for iron-doped perovskites (15). Such thermal lattice vibrations are also induced by illuminating the samples with white light. In this case the long wavelength part of the radiation (IR) is responsible for the activation. The $g' \approx 18$ signal changes in the same manner as observed at elevated temperatures (Fig. 8).

Above 650 K the temperature dependence of the $g' \approx 18$ signal becomes irreversible. Thermal diffusion leads by compensation of the vacancies and redox processes to the disappearance of the low field signal (Fig. 9, Table 4). In an oxygen atmosphere this process is superimposed by the uptake of oxygen which is converted into oxide ions filling the oxygen vacancies. Thus, the coordination sphere of the appropriate Fe^{3+} ions is saturated. It becomes more symmetric and the centres contribute to the ESR signal at $g' \approx 2$, the intensity of which rises as the low field line decreases. The reverse behavior of the $g' \approx 2$ line is observed in nitrogen atmosphere and *in vacuo*, respectively, and can be explained in terms of line broadening due to thermally induced lattice distortions. In addition, reduction processes, such as the capture of the electrons in the vacancies by V^{4+}, have to be taken into account as a reason for the intensity decrease in the $g' \approx 2$ line.

The relatively high resistance of the Fe^{3+}–$V_O(e^-)$ centres against temperature indicates that the electrons captured by the vacancies occupy a low energy level. This is also supported by the results of conductivity measurements described above. It was found that the electrical conductivity of catalyst V : Fe = 1 : 1.4 decreases on cesium doping (Fig. 1). An explanation of this observation can be given if one assumes that the defect centres in the doped catalysts remove electrons from the conduction band, thus lowering the number of charge carriers available for the conduction. The higher activation energy for

the doped catalyst (Fig. 2) suggests that the electrons trapped in the vacancies have energies below that of the other donor levels so that they can escape only at higher temperatures. The energy of the donor level depends on its number of electrons. With increasing oxygen pressure more and more electrons are removed from the donor level. Thus, the donor level is lowered energetically and the activation energy of the electrical conductivity rises (Fig. 2).

As expected, the lattice vacancies are also compensated for by the application of high mechanical pressure (Fig. 10). The reduced intensity of the $g' \approx 18$ signal indicates that neighbouring oxide ions are pushed toward the vacancy under pressure. Thus, the local environment of the Fe^{3+} ions is modified and a very broad signal at $g' > 2$ arises from these ions. When the pressure is removed the oxide ions return to their initial position.

The results of temperature- and pressure-dependent ESR measurements discussed above support the assignment of the $g' \approx 18$ line to oxygen vacancies in the neighbourhood of Fe^{3+} ions which are occupied by an electron.

From the Mössbauer spectrum of sample V : Fe : Cs = 1 : 1.4 : 0.06 (Fig. 5) it could be derived that the catalyst consists of about 42% α-Fe_2O_3, 32% $FeVO_4$, and 26% $Fe_xV_yO_z$ (Table 2). However, potentiometric titration (20) revealed that the solid contains oxidizable components. Since no Fe^{2+} was detected in the Mössbauer spectra it was assumed that V^{5+} must have been reduced to V^{4+}, a reaction which is frequently observed in V_2O_5-based catalysts (21). Thus, 47% of the overall vanadium content is present as V^{4+}. On the basis of these results the formal composition of the catalyst V : Fe : Cs = 1 : 1.4 : 0.06 can be written as 0.53 V_2O_5, 0.47 V_2O_4, 1.4 Fe_2O_3, and 0.06 Cs_2SO_4. Assuming that 32% Fe_2O_3 reacts with the appropriate amount of V_2O_5 to $FeVO_4$, the following composition can be calculated:

$$0.59\alpha\text{-}Fe_2O_3 \cdot 0.90\ FeVO_4 \cdot (0.08\ V_2O_5 \cdot 0.47\ V_2O_4 \cdot 0.36\ Fe_2O_3) \cdot 0.06\ Cs_2SO_4.$$

In a similar manner the composition of the catalyst V : Fe : Cs = 1 : 1 : 0.06 was estimated. Mössbauer measurements revealed that the solid consists of about 45% α-Fe_2O_3, 39% $Fe_2V_4O_{13}$, and 16% $Fe_xV_yO_z$ (Table 2). By potentiometric titration (20) a percentage of 23% V^{4+} was determined. Accordingly, the formal composition of the catalyst is

$$0.45\alpha\text{-}Fe_2O_3 \cdot 0.39\ Fe_2V_4O_{13} \cdot (0.16\ Fe_2O_3 \cdot 0.23\ V_2O_4) \cdot 0.06\ Cs_2SO_4.$$

For both cesium-doped catalysts the components in parentheses apparently form the $Fe_xV_yO_z$ phases which cause the ESR signals at $g' \approx 18$. Setting the vanadium content to unity their approximate formal composition can be written as

for V : Fe : Cs = 1 : 1.4 : 0.06,

$$Fe_{0.65}VO_{3.14};$$

V : Fe : Cs = 1 : 1 : 0.06,

$$Fe_{0.70}VO_{3.04}.$$

The Fe : V : O ratios, which are very similar but not identical, suggest that these phases are nonstoichiometric. The degree of reduction indicates an oxygen deficit which is obviously caused by oxygen lattice vacancies. The ESR signal of V^{4+} is expected to occur in the $g' < 2$ region (13). However, it is not resolved due to superposition with the signals of $FeVO_4$ and $Fe_2V_4O_{13}$, respectively, and line broadening caused by magnetic exchange interactions.

The above interpretation is supported by the good fit of experimental and simulated ESR spectra for the sample V : Fe : Cs = 1 : 1 : 0.06 in both X-band and Q-band using the same parameter set (Fig. 6). The calculated spectrum was obtained by superposition of five lines with the following parameters assuming Gaussian lineshape

1. $S = 5/2$, $g_{iso} = 2.00$, $D = 4800$ MHz, $a = 960$ MHz, $\Delta B = 10.0$ mT (for Fe^{3+}–$V_O(e^-)$);
2. $S = 5/2$, $g_{iso} = 2.00$, $D = 4000$ MHz, $a = 800$ MHz, $\Delta B = 50.0$ mT (for Fe^{3+}–$V_O(e^-)$);
3. $S = 5/2$, $g_{iso} = 2.00$, $D = 3600$ MHz, $a = 720$ MHz, $\Delta B = 50.0$ mT (for Fe^{3+}–$V_O(e^-)$);
4. $S = 5/2$, $g_{iso} = 2.10$, $D = 0$, $a = 0$, $\Delta B = 55.0$ mT (for $Fe_2V_4O_{13}$);
5. $S = 5/2$, $g_{iso} = 1.96$, $\Delta B = 25.0$ mT (for V^{4+}).

On the other hand, it cannot be excluded that the phases $Fe_xV_yO_z$ contain V^{5+} and V^{3+} side by side; the latter are, however, observable only at very low temperatures (<4 K). In order to achieve a satisfactory fit of experimental and calculated ESR spectra in the range between $g' \approx 18$ and $g' \approx 2$ (Fig. 6) it was necessary to superpose two broad Fe^{3+} signals with $D = 4000$ and 3600 MHz, respectively. This means that for the Fe^{3+}–$V_O(e^-)$ centres a certain distribution of D and a has to be assumed indicating that the local symmetry of the iron coordination sphere is not exactly the same for each centre. In addition to the high concentration of lattice defects, this distribution distorts the structure and is probably another reason why

the $Fe_xV_yO_z$ phases are amorphous and catalytically active.

One has to keep in mind that the formulae of the $Fe_xV_yO_z$ components written above only represent the gross composition of the new phases which were derived from the proportion of the catalyst constituents. Formally, the phase $Fe_{0.70}VO_{3.04}$ can be regarded as consisting of $2x$ VO_2 + $(1 - x)$ Fe_2O_3 with $x = 0.59$. Such compositions were observed as intermediates during the oxidation of solid solutions of V_2O_3 and α-Fe_2O_3 (22) according to the equation

$$\begin{array}{l} Fe_{2(1-x)}V_{2x}O_3 \xrightarrow{(x/2)O_2} 2xVO_2 + (1-x)Fe_2O_3 \quad (0 < x < 1) \\ \qquad\qquad\qquad\qquad \downarrow {\scriptstyle (x/2)O_2} \\ \qquad\qquad\qquad\qquad xV_2O_5 + (1-x)Fe_2O_3. \end{array} \qquad [7]$$

Without a doubt, further investigations are certainly necessary to elucidate the particular structure of the $Fe_xV_yO_z$ phases and the role of cesium. It seems likely that this large, easily polarizable cation is needed to stabilize the lattice vacancies in its neighborhood, which occur in relatively high concentration and obviously make this phase nonstoichiometric. Nonstoichiometry owing to lattice defects is a frequently observed feature in slightly reduced *n*-type semiconducting oxides like V_2O_5 (21) and measurements of the electrical conductivity confirmed that the catalysts under study are, in fact, *n*-type semiconductors.

In addition to catalysts V : Fe : Cs = 1 : 1 : 0.06 and 1 : 1.4 : 0.06, another one with a molar ratio of 1 : 1.4 : 0.12 was examined by ESR spectroscopy. It showed the same $g' \approx 18$ signal intensity as the sample 1 : 1.4 : 0.06. This result indicates that the formation of the new phase is to a large extent independent of the cesium amount as long as the cesium concentration does not fall below a certain minimum.

2. *Catalytic Behaviour*

For the beneficial effect of cesium doping on catalyst selectivity a rather complex combination of various influences has to be discussed. It has been found that the surface acidity of the catalyst is diminished by doping them with cesium and by increasing iron content (Table 1). In contrast, the selectivity increases in the same order (Fig. 11). The reason may be that the reduced surface acidity lowers the adsorption strength of the basic hydrocarbon molecules and their interaction period with the surface. Thus, the inner ring oxidation product 9-fluorenone is easily desorbed from the surface and further reaction to phthalic anhydride or even to the carbon oxides can be prevented.

On the other hand, the high yield of selective oxidation products over iron-rich cesium-doped catalysts indicates that nucleophilic addition of O^{2-} is the preferred reaction mechanism (17). As discussed above, experimental results of ESR, Mössbauer, and XRD measurements revealed that in cesium-doped catalysts with increasing iron content an amorphous phase is formed which contains Fe^{3+}–$V_O(e^-)$ defects. The relative percentage of this phase with respect to the overall iron content of the catalyst increases from zero (V : Fe = 1 : 0.13) to 26% (V : Fe = 1 : 1.4) (Table 2). In the same direction the 9-fluorenone selectivity is enhanced from 83 to 99% (Fig. 11). So it seems likely that there is a close relationship between the appearance of the new $Fe_xV_yO_z$ phase and that part of the selectivity which goes beyond the enhancement caused by the reduced surface acidity. The $V_O(e^-)$ defects are electron donor centres which can react with adsorbed gas phase oxygen in the following manner (17):

$$O_2(\text{surface}) + e^- + \square \rightarrow O_2^-(\text{surface})$$

$$O_2^-(\text{surface}) + e^- + \square \rightarrow O_2^{2-}(\text{surface}) \rightarrow 2\ O^-(\text{surface})$$

$$2\ O^-(\text{surface}) + 2\ e^- \rightarrow 2\ O^{2-}(\text{surface}).$$

The increase in the $g' \approx 2$ ESR intensity at the expense of the $g' \approx 18$ signal after calcining the catalysts in oxygen atmosphere (Fig. 8, Table 4) indicates the occurrence of such a process. In addition it has been observed that the oxygen uptake of samples V : Fe : Cs = 1 : 1 : 0.06 and 1 : 1.4 : 0.06 which contain the phase $Fe_xV_yO_z$ rises markedly in comparison to catalysts in which this phase is not present (Table 1). Accordingly, nucleophilic O^{2-} ions are formed at the surface probably in a position very close to the adsorbed hydrocarbon molecules. These oxide ions are known to be suitable for insertion into the hydrocarbon molecule and not to cause total oxidation as O_2^- and O^- do (17). The preferred formation of O^{2-} on the cesium-doped catalysts is also strongly supported by the exponent *n* of the electrical conductivity dependence on oxygen pressure.

The ESR measurements of *in situ* reaction with fluorene revealed that a radical derived from the aromatic is formed at elevated temperatures over certain catalysts. The extent of radical formation is highest when the V^{5+} = O bond is exposed to the surface, for example, in the case of pure V_2O_5 and β-$VOPO_4$ (Table 5). From XRD measurements it is known that V_2O_5 is the main component of the catalysts V : Fe = 1 : 0.13 and V : Fe : Cs = 1 : 013 : 0.06. Accordingly, the radical signal is much more intensive than for the iron-rich catalysts with a ratio of V : Fe = 1 : 1.4. In the case of the undoped sample V : Fe = 1 : 0.13 having the lowest 9-fluorenone selectiv-

ity, it reaches even the intensity over pure V_2O_5. If free radicals are formed during catalytic oxidation of fluorene they could easily react with gaseous molecular oxygen to give unstable peroxide intermediates which decompose in a series of consecutive steps eliminating singlet oxygen which is very reactive and, in fact, can lead to total oxidation (23):

$$R\text{H} + \text{V}^{5+} = \text{O} \rightarrow R\cdot + \text{V}^{4+}\text{—OH}$$

$$R\cdot + \text{O}_2 \rightarrow R\text{-O-O}\cdot$$

$$2\ \text{R-O-O}\cdot \rightarrow R\text{-O-O-O-O-}R \rightarrow 2\ R\text{-O}\cdot + \text{O}_2(\text{singlet}).$$

Although such a reaction pathway is rather favoured in homogeneous catalysis (21) the results indicate that it possibly might be involved in heterogeneous catalysis as well. Thus, it could be a reason why the catalysts with a ratio V : Fe = 1 : 0.13 have the lowest selectivities.

CONCLUSIONS

When V_2O_5–Fe_2O_3 catalysts are doped with Cs_2SO_4, the 9-fluorenone selectivity increases markedly in the catalytic oxidation of fluorene. For this effect mainly two reasons are assumed to be responsible:

1. Cesium dopants reduce surface acidity of the catalysts and weaken the adsorptive bonding of the basic ring systems on the surface. Thus, the desorption of the selectively oxidized hydrocarbon molecules is facilitated and total oxidation is prevented.

2. In cesium-doped V_2O_5–Fe_2O_3 catalysts, amorphous nonstoichiometric phases are formed with increasing iron content. In catalysts with an atomic ratio of V : Fe : Cs = 1 : 1 : 0.06 and 1 : 1.4 : 0.06 these phases have approximate formal compositions of $Fe_{0.70}VO_{3.04}$ and $Fe_{0.65}VO_{3.14}$, respectively. They contain Fe^{3+} ions with an oxygen vacancy in their coordination sphere being occupied by an electron. The cesium ions probably stabilize the oxygen defects.

The described vacancies are assumed to act as active sites in the selective oxidation reaction by adsorbing and converting gas phase oxygen rapidly to O^{2-}, which is suitable for the nucleophilic addition to the hydrocarbon molecule, while the reduced surface acidity leads to fast desorption of the oxygenate selectively formed.

In the case of iron-poor catalysts with a ratio V : Fe = 1 : 0.13 these two beneficial influences on 9-fluorenone selectivity are probably compensated for to a certain degree by a radical mechanism acting rather nonselectively.

REFERENCES

1. Odening, B., Käßner, P., and Baerns, M., *in* "Proceedings, DGMK Conference on Selective Oxydation in Petrochemistry, Goslar, Germany," p. 347.
2. Baerns, M., Borchert, H., Kalthoff, R., Käßner, P., and Majunke, F., *Stud. Surf. Sci. Catal.* **72,** 57 (1992).
3. Toubol, M., and Popot, A., *J. Therm. Anal.* **31,** 117 (1986).
4. Toubol, M., and Ingrain, D., *J. Less-Common Met.* **71,** 55 (1980).
5. Haul, R., and Dümbgen, G., *Chem.-Ing.-Tech.* **32,** 349 (1960); **35,** 586 (1963).
6. Wagner, C. D., Riggs, W. M., Davis, L. E., Moulder, J. F., and Mullenberg, G. E., (Eds.), "Handbook of X-Ray Photoelectron Spectroscopie." Perkin–Elmer Corp., Eden Prairie, MN, 1978.
7. Borchert, H., Ph.D. Thesis, Ruhr-Universität Bochum, 1993.
8. Wertz, J. E., and Bolton, J. R., "Electron Spin Resonance: Elementary Theory and Practical Applications." McGraw–Hill, New York, 1972.
9. Pilbrow, J. R., "Transition Ion Electron Paramagnetic Resonance." Clarendon, Oxford, 1990.
10. Baerns, M., Kalthoff, R., Käßner, P., and Zein, A., "Katalyse," DECHEMA Monographie (H. Kral and D. Behrens, Eds.), Vol. **118,** Verlag Chemie, Weinheim, 1989.
11. Zein, A., and Baerns, M., *J. Chromatogr. Sci.* **27,** 249 (1989).
12. Szabo, Z. G., and Kallo, D., "Contact Catalysis." Vol. 1, Elsevier, Amsterdam/Oxford/New York, 1976.
13. Chand, P., Jain, V. K., and Upreti, G. C., *Magn. Reson. Rev.* **14,** 49 (1988).
14. Aasa, R., *J. Chem. Phys.* **52,** 3919 (1970).
15. Murugaraj, P., and Kutty, T. R. N., *J. Mater. Sci. Lett.* **5,** 171 (1986).
16. "Handbook of Chemistry and Physics," 72nd ed. CRC Press, Boca Raton/Ann Arbor/Boston, 1991–1992.
17. Libre, J. M., Parbaux, B., Grzybowska, B., Conflant, P., and Bonnelle, J. P., *Appl. Catal.* **6,** 315 (1983).
18. Possenriede, E., Schirmer, O. F., and Donnerberg, H. J., *Ferroelectrics* **92,** 245 (1989).
19. Possenriede, E., Schirmer, O. F., Donnerberg, H. J., and Hellermann, B., *J. Phys. Condens. Matter* **1,** 7267 (1989).
20. Niwa, M., and Murakami, Y., *J. Catal.* **76,** 9 (1982).
21. Bielanski, A., and Haber, J., "Oxygen in Catalysis." Dekker, New York/Basel/Hong Kong, 1991.
22. Stander, P. P., and van Vuuren, C. P. J., *Thermochim. Acta* **157,** 347 (1990).
23. Höver, H., "Problems in Organic Reaction Mechanisms." Wiley, New York, 1970.